J|A|C|S
ARTICLES
Published on Web 02/20/2003

# On the Dissolution Processes of $Na_2I^+$ and $Na_3I_2^+$ with the Association of Water Molecules: Mechanistic and Energetic Details

Qiang Zhang, Catherine J. Carpenter, Paul R. Kemper, and Michael T. Bowers*

*Contribution from the Department of Chemistry and Biochemistry, University of California, Santa Barbara, California 93106-9510*

Received September 4, 2002; E-mail: bowers@chem.ucsb.edu

***Abstract:*** The sequential association energies for one through six water molecules clustering to $Na_2I^+$, as well as one and two water molecules clustering to $Na_3I_2^+$, are measured. The association energies show a pairwise behavior, indicating a symmetric association of water molecules to the linear $Na_2I^+$ and $Na_3I_2^+$ ions. This pairwise behavior is well reproduced by Density Functional Theory (DFT) calculations. DFT calculations also suggest that a significant separation of charge for the Na−I ion pair occurs when four or more water molecules cluster to a single sodium center. Two different solvent-separated ion pairs have been identified with the DFT calculations. Experiments also show that the dissolution processes, loss of a neutral NaI unit, occurs when six or more water molecules have been added to $Na_2I^+$ cluster. However, one or two water molecules are able to detach an NaI unit from the $Na_3I_2^+$ cluster. The difference in solubility of the $Na_2I^+$ and $Na_3I_2^+$ ions is due to the difference in the energies required to lose an NaI unit from these two species. The experiment also confirms that the loss of a neutral NaI unit, instead of an $Na^+$ ion, occurs during the dissolution processes of $Na_3I_2^+$. The microsolvation schemes proposed to explain our experimental observations are supported by DFT and phase space theory (PST) calculations.

## Introduction

The dissolution of sea salt particles, MX (M = alkali elements and X = halide elements), is a common occurrence in nature. When a sea salt crystal comes into contact with water, the surface of the salt crystal is covered with water molecules. Charge separation is then induced by the polar water molecules, forming partially charged $M^{\delta+}$ and $X^{\delta-}$ ion pairs at the surface of the crystal. When the free energy of hydration exceeds the free energy of the lattice, the hydrated $M^+$ and $X^-$ ions leave the bulk solid phase and disperse into the aqueous phase.[1,2] From simple saturation concentration considerations, it has been determined that at room temperature, nine water molecules are required to dissolve an NaCl unit and only about five water molecules for an NaI unit. Despite our familiarity with this phenomenon, the true picture of the dissolution processes is not clear from the microscopic point of view. In particular, the question of whether MX leaves the lattice surface as a unit or separately as $M^+$ and $X^-$ is in doubt and remains open to discussion.[3]

The dissolution of sea salt particles can also take place in the gas phase, playing an important role in environmental and atmospheric chemistry.[4,5] It is known that small sea salt particles are brought into the gas phase by wave action in the marine boundary layer and in coastal regions. The halogen anions ($X^-$) contained in sea salt particles can destroy ozone ($O_3$), a key tropospheric oxidant and greenhouse gas, via photochemical reactions. The most recent research reveals that the reactions of $O_3$ with aqueous sea salt ions control the chemistry at the air−water interface,[6] yet the details of the microsolvation processes of the small sea salt cluster ions in the gas phase remain unknown.

The association reactions of water molecules with alkali cations[7,8] and halide anions[9,10] have been widely investigated both experimentally and theoretically.[11] Small alkali halide−water ions have also been observed in the gas phase.[12] Both experimental[13,14] and theoretical[15−22] studies for the dissolu-

(1) Brown, T. L.; LeMay, H. E.; Bursten, B. E. *Chemistry, The Central Science* (Chapter 13); Prentice Hall: New Jersey, 1997.
(2) Harned, H. S.; Owen, B. B. *The Physical Chemistry of Electrolytic Solutions*; Reinhold: New York, 1958.
(3) Yamabe, S.; Kouno, H.; Matsumura, K. *J. Phys. Chem. B* **2000**, *104*, 10 242.
(4) Oum, K. W.; Lakin, M. J.; DeHaan, D. O.; Brauers, T.; Finlayson-Pitts, B. J. *Science* **1998**, *279*, 74.
(5) Schweitzer, F.; Magi, L.; Mirabel, P.; George, C. *J. Phys. Chem. A* **1998**, *102*, 593.
(6) Knipping, E. M.; Lakin, M. J.; Foster, K. L.; Jungwirth, P.; Tobias, D. J.; Gerber, R. B.; Dabdub, D.; Finlayson-Pitts, B. J. *Science*, **2000**, *288*, 301.
(7) (*a*) Dalleska, N. F.; Tjelta, B. L.; Armentrout, P. B. *J. Phys. Chem.* **1994**, *98*, 4191. (*b*) Marinelli, P. J.; Squires, R. R. *J. Am. Chem. Soc.* **1989**, *111*, 4101. (*c*) Dzidic, I.; Kebarle, P. *J. Phys. Chem.* **1970**, *74*, 1466.
(8) (*a*) Hashimoto, K.; Morokuma, K. *J. Am. Chem. Soc.* **1994**, *116*, 11 436. (*b*) Bauschlicher, C. W.; Langhoff, S. R.; Patridge, H.; Rice, J. E.; Komornicki, A. *J. Chem. Phys.* **1991**, *95*, 5142.
(9) (*a*) Davis, A. V.; Zanni, M. T.; Weinkauf, R.; Neumark, D. M. *Chem. Phys. Lett.* **2002**, *353*, 455. (*b*) Ayotte, P.; Weddle, G. H.; Johnson, M. A. *J. Chem. Phys.* **1999**, *110*, 7129. (*c*) Choi, J. H.; Kuwata, K. T.; Cao, Y. B.; Okumura, M. *J. Phys. Chem. A* **1998**, *102*, 503. (*d*) Markovich, G.; Pollack, S.; Giniger, R.; Cheshnovsky, O. *J. Chem. Phys.* **1994**, *101*, 9344. (*e*) Hiraoka, K.; Mizuse, S.; Yamabe, S. *J. Phys. Chem.* **1988**, *92*, 3943. (*f*) Arshadi, M.; Yamdagni, R.; Kebarle, P. *J. Phys. Chem.* **1970**, *74*, 1475.
(10) (*a*) Lee, H. M.; Kim, D.; Kim, K. S. *J. Chem. Phys.* **2002**, *116*, 5509. (*b*) Vila, F. D.; Jordan, K. D. *J. Phys. Chem. A* **2002**, *106*, 1391. (*c*) Chen, H. Y.; Sheu, W. S. *J. Am. Chem. Soc.* **2000**, *122*, 7534. (*d*) Gai, H. D.; Schenter, G. K.; Dang, L. X.; Garrett, B. C. *J. Chem. Phys.* **1996**, *105*, 8835. (*e*) Serxner, D.; Dessent, C. E. H.; Johnson, M. A. *J. Chem. Phys.* **1996**, *105*, 7231.

tion of NaCl with water molecules have been reported. It is found that two intermediate states, the contact ion pair (CIP) and the solvent-separated ion pair (SSIP), exist prior to the dissolution of NaCl. However, the details of the dissolution process are not yet fully understood. In particular, the minimum number of water molecules required for the dissolution to take place has not been determined.

Our goal in this work is to explore the sea salt dissolution process using a combination of experimental and theoretical methods.[11a,23] In particular, we will measure the binding energies between the salt cluster ions and neutral water ligands and explore the dissolution reaction mechanisms. We chose NaI as our first system to study because it is monoisotopic and is predicted to take fewer water molecules than NaCl to effect solvation. Our findings follow.

## Experimental Methods

Experimental details of the method and instrument have been published previously.[24−26] Briefly, the $Na(NaI)^+_{n=1,2}$ cations are formed by laser vaporization of a sodium iodide rod in a helium buffer gas. The pulsed 308 nm XeCl excimer laser is typically run at 10 Hz with a power of 300−400 mJ per pulse. The desorbed salt plasma is entrained in a high-pressure pulse of He that cools the plasma and induces cluster formation. The timing of the He pulse is synchronized with the laser pulse using a home-built delay generator. Typically, the He pulse width is 200−600 $\mu$s with a backing pressure of 60 Psi. The bare $Na(NaI)^+_{n=1,2}$ ions are mass selected by a quadrupole mass filter and injected into a drift reaction cell containing a mixture of He and $H_2O$. Typically, the composition of the reaction gas is 3 Torr of He and 0.01−0.5 Torr of water vapor. The vapor pressure of water is measured by a barometer that is calibrated by a residual gas analyzer. The cell temperature is varied from 200 to 600 K. Ions exiting the drift cell pass through a second quadrupole mass analyzer and are detected using single-ion counting methods. The ions in the reaction cell drift under the influence of a weak electric field that does not measurably perturb their thermal energies. The following equilibria are rapidly established

$$Na(NaI)^+_{n=1,2}(H_2O)_{m-1} + H_2O \underset{k_{-1}}{\overset{k_1}{\rightleftharpoons}} Na(NaI)^+_{n=1,2}(H_2O)_m \quad (1)$$

When the number of associated water molecules reaches a threshold value, $x + y$, dissolution occurs and fragmentation of parent ions is observed (reaction 2)

$$Na(NaI)^+_{n=1,2}(H_2O)_{x+y} \xrightarrow{k_d} Na(NaI)^+_{n=0,1}(H_2O)_x + (NaI)(H_2O)_y \quad (2)$$

The reactant and product ions are mass analyzed by the second quadrupole as mentioned above.

The measured intensities of the various $Na(NaI)^+_{n=1,2}(H_2O)_m$ ions are used to determine the equilibrium constants

$$K_p^0 = \frac{[Na(NaI)^+_{n=1,2}(H_2O)_m]\cdot(760)}{[Na(NaI)^+_{n=1,2}(H_2O)_{m-1}]\cdot P_{H_2O}} \quad (3)$$

where $P_{H_2O}$ is the pressure of $H_2O$ in Torr and (760) Torr normalizes the $K_p^0$ values to standard state conditions. The standard-state free energies are then calculated using eq 4

$$\Delta G_T^0 = -RT \ln K_p^0 \quad (4)$$

and enthalpies and entropies are determined by plotting $\Delta G_T^0$ vs $T$

$$\Delta G_T^0 = \Delta H_T^0 - T\Delta S_T^0 \quad (5)$$

where $\Delta H_T^0$ and $-\Delta S_T^0$ are the intercept and the slope of the plot, respectively. These quantities are valid over the temperature range of the experiment. To obtain true bond dissociation energies ($D_0 \equiv -\Delta H_0^0$), extrapolations of $\Delta H_T^0$ to 0 K using statistical mechanics methods are performed.[27] The geometry parameters and vibrational frequencies determined with DFT are used in the extrapolations.

## Theoretical Methods

Candidate structures and energies were obtained with the Density Functional Theory (DFT) method using the unrestricted open shell B3LYP functional parametrization.[28,29] All calculations were carried out on an SGI IRIX 64 workstation with the GAUSSIAN98 package.[30] For sodium, oxygen, and hydrogen, the built-in 6-311++G** basis was used. For iodine, we used the quasi-relativistic 7-valence-electron effective core potential (ECP) developed by the Stuttgart group, which uses a relativistic ECP to replace the 46-electron [Kr + $4d^{10}$] core and a [2$s$3$p$] contraction of (4$s$5$p$) primitive set to represent the valence electrons.[31] Full geometry optimizations were achieved for all species involved in this work. Corrections for zero point energy (ZPE) and basis set superposition error (BSSE) were also performed.

The kinetics and dynamics of the dissolution reactions were studied with statistical phase space theory (PST).[32−38] Specifically, PST was used to calculate the efficiencies for reactions


(11) (*a*) Weis, P.; Kemper, P. R.; Bowers, M. T.; Xantheas, S. S. *J. Am. Chem. Soc*. **1999**, *121*, 3531. (*b*) Ayotte, P.; Nielsen, S. B.; Weddle, G. H.; Johnson, M. A.; Xantheas, S. S. *J. Phys. Chem. A* **1999**, *103*, 10 665. (*c*) Cabarcos, O. M.; Weinheimer, C. J.; Lisy, J. M.; Xantheas, S. S. *J. Chem. Phys*. **1999**, *110*, 5.
(12) Grégoire, G.; Mons, M.; Dimicoli, I.; Dedonder-Lardeux, C.; Jouvet, C.; Martrenchard, S.; Solgadi, D. *J. Chem. Phys*. **2000**, *112*, 8794.
(13) Peslherbe, G. H.; Ladanyi, B. M.; Hynes, J. T. *J. Phys. Chem. A* **1998**, *102*, 4100.
(14) Ault, B. S. *J. Am. Chem. Soc*. **1978**, *100*, 2426.
(15) Dedonder-Lardeux, C.; Grégoire, G.; Jouvet, C.; Martrenchard, S.; Solgadi, D. *Chem. Rev*. **2000**, *100*, 4023.
(16) Jungwirth, P. *J. Phys. Chem. A* **2000**, *104*, 145.
(17) Petersen, C. P.; Gordon, M. S. *J. Phys. Chem. A* **1999**, *103*, 4162.
(18) Stefanovich, E. V.; Truong, T. N. *J. Chem. Phys*. **1996**, *104*, 2946.
(19) Barnett, R. N.; Landman, U. *J. Phys. Chem*. **1996**, *100*, 13 950.
(20) Woon, D. E.; Dunning, Jr., T. H. *J. Am. Chem. Soc*. **1995**, *117*, 1090.
(21) Asada, T.; Nishimoto, K. *Chem. Phys. Lett*. **1995**, *232*, 518.
(22) Smith, D. E.; Dang. L. X. *J. Chem. Phys*. **1994**, *100*, 3757.
(23) (*a*) Bushnell, J. E.; Kemper, P. R.; Bowers, M. T. *J. Phys. Chem.* **1994**, *98*, 2044. (*b*) Kemper, P. R.; Bushnell, J.; von Helden, G.; Bowers, M. T. *J. Phys. Chem.* **1993**, *97*, 52.
(24) Weis, P.; Kemper, P. R.; Bowers, M. T. *J. Phys. Chem. A* **1997**, *101*, 8207.
(25) Kemper, P. R.; Weis, P.; Bowers, M. T. *Int. J. Mass. Spectrom. Ion Processes* **1997**, *160*, 17.
(26) Bushnell, J. E.; Kemper, P. R.; Maître, P.; Bowers, M. T. *J. Am. Chem. Soc*., **1994**, *116*, 9710.
(27) Kemper, P. R.; Bushnell, J.; van Koppen, P.; Bowers, M. T. *J. Phys. Chem*. **1993**, *97*, 1810.
(28) Stephens, P. J.; Devlin, F. J.; Chabalowski, C. F.; Frisch, M. J. *J. Phys. Chem*. **1994**, *98*, 11 623.
(29) Becke, A. D. *J. Chem. Phys*. **1993**, *98*, 5648.
(30) Frisch, M. J.; Trucks, G. W.; Schlegel, H. B.; Scuseria, G. E.; Robb, M. A.; Cheeseman, J. R.; Zakrzewski, V. G.; Montgomery, J. A.; Stratmann, Jr., R. E.; Burant, J. C.; Dapprich, S.; Millam, J. M.; Daniels, A. D.; Kudin, K. N.; Strain, M. C.; Farkas, O.; Tomasi, J.; Barone, V.; Cossi, M.; Cammi, R.; Mennucci, B.; Pomelli, C.; Adamo, C.; Clifford, S.; Ochterski, J.; Petersson, G. A.; Ayala, P. Y.; Cui, Q.; Morokuma, K.; Malick, D. K.; Rabuck, A. D.; Raghavachari, K.; Foresman, J. B.; Cioslowski, J.; Ortiz, J. V.; Baboul, A. G.; Stefanov, B. B.; Liu, G.; Liashenko, A.; Piskorz, P.; Komaromi, I.; Gomperts, R.; Martin, R. L.; Fox, D. J.; Keith, T.; Al-Laham, M. A.; Peng, C. Y.; Nanayakkara, A.; Gonzalez, C.; Challacombe, M.; Gill, P. M. W.; Johnson, B.; Chen, W.; Wong, M. W.; Andres, J. L.; Gonzalez, C.; Head-Gordon, M.; Replogle, E. S.; Pople, J. A. *Gaussian 98*, revision A.5; Gaussian, Inc.: Pittsburgh, PA, 1998.
(31) Kaupp, M.; Schleyer, P. v. R.; Stoll, H.; Preuss, H. *J. Am. Chem. Soc*. **1991**, *113*, 6012.
(32) (*a*) Graul, S. T.; Carpenter, C. J.; Bushnell, J. E.; van Koppen, P. A. M.; Bowers, M. T. *J. Am. Chem. Soc*. **1998**, *120*, 6785. (*b*) Bass, L. M.; Bowers, M. T. *J. Chem. Phys*. **1987**, *86*, 2611. (*c*) Illies, A. J.; Jarrold, M. F.; Bass, L. M.; Bowers, M. T. *J. Am. Chem. Soc*. **1983**, *105*, 5775. (*d*) Su, T.; Bowers, M. T. *J. Chem. Phys*. **1973**, *58*, 3027.

1 and 2. A brief summary of the PST calculations is available in the Supporting Information along with the input parameters (geometries, vibrational frequencies, and relative energetics) adopted from the DFT calculations.

The reaction efficiency at temperature $T$, $\omega(T)$, is the fraction of reactant collisions that result in product formation. It is defined as $k_{expt}(T)/k_{coll}(T)$, where $k_{expt}(T)$ is the experimentally observed rate constant and $k_{coll}(T)$ is the collision rate constant for reactants. The intermediate adducts $Na(NaI)^{+}_{n=1,2}(H_2O)_m$ are assumed to be formed in the steady state at the collision rate of the reactants (i.e., $k_1 = k_{coll}$)

$$Na(NaI)^{+}_{n=1,2}(H_2O)_{m-1} + H_2O \underset{k_{-1}(T)}{\overset{k_1(T)}{\rightleftharpoons}} Na(NaI)^{+}_{n=1,2}(H_2O)_m \xrightarrow{k_d(T)} Na(NaI)^{+}_{n=0,1}(H_2O)_x + (NaI)(H_2O)_y \quad (6)$$

This allows the reaction efficiency to be rewritten as follows

$$\omega(T) = \frac{k_{expt}(T)}{k_{coll}(T)} = \frac{k_d(T)}{k_d(T) + k_{-1}(T)} \quad (7)$$

The right-hand side of eq 7 was calculated with PST (see the Supporting Information) and because $k_{coll}(T)$ can be calculated with Average Dipole Orientation Theory,[32a] $k_{expt}(T)$ can be obtained. These calculated $k_{expt}(T)$ values were used to determine extents of reaction (eq 8) under the conditions of our experiment

$$\frac{[Na(NaI)^{+}_{n=1,2}(H_2O)_{m-1}]}{[Na(NaI)^{+}_{n=1,2}(H_2O)_{m-1}]_0} = e^{-k_{expt}(T)P_{H_2O}t} \quad (8)$$

where $t$ is time. The extent-of-reaction values calculated in eq 8 were used to evaluate the mass spectra measured in this study.

## Results and Discussion

**1. Dissolution of Salt Clusters.** Both the equilibrium between $Na(NaI)_n^+$ and water molecules (reaction 1) and the dissolution of $Na(NaI)_n^+$ by the association of water molecules (reaction 2) are observed in our experiments. Figure 1 shows the room-temperature mass spectra recorded for $Na_2I^+$ at different water vapor pressures. The bottom panel was recorded without any water added to the reaction cell. Only a single $Na_2I^+$ peak is observed. When the water pressure is raised to 0.01 Torr, a nonequilibrium distribution of up to four water molecules associating to an $Na_2I^+$ core is observed, as well as a small peak for $Na_2I^+(H_2O)_5$. When the pressure of water is increased to 0.07 Torr, equilibrium is established for the $Na_2I^+(H_2O)_m$ series of ions with peaks for as many as six $H_2O$ ligands clustering to $Na_2I^+$ observed. In addition, $Na^+(H_2O)_x$ ions appear with $x = 3$ and 4. These species are also in equilibrium with $H_2O$. The top spectrum was recorded with a water vapor pressure of 0.31 Torr. At this water pressure, more $Na(H_2O)_x^+$ fragments are formed and dominate the spectrum.

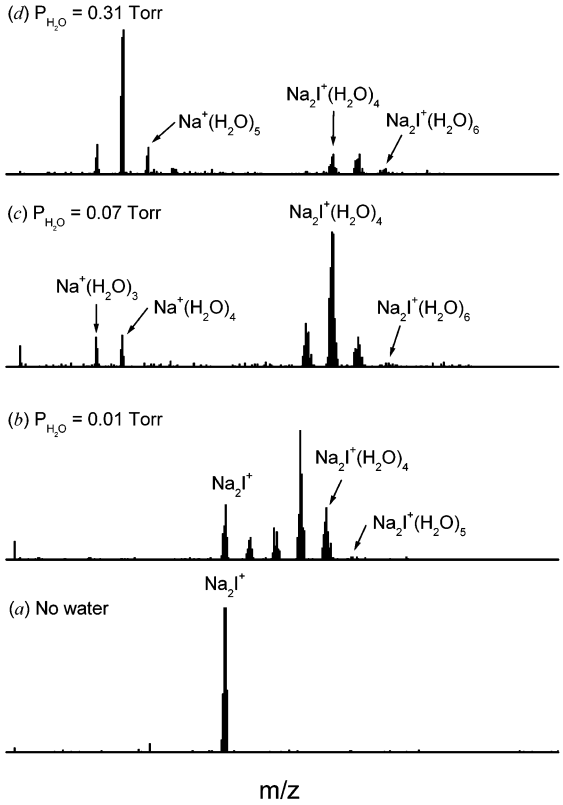


***Figure 1.*** Mass spectra of $Na_2I^+$ with different water pressures at room temperature. The dissolution species $Na^+(H_2O)_x$, appear when the $Na_2I^+(H_2O)_6$ adduct is formed.

As shown by the spectra in Figure 1, no dissolution processes are observed as long as the number of water molecules associated to $Na_2I^+$ is less than six. Analogous experiments were carried out for the $Na_3I_2^+$ ion with the mass spectra shown in Figure 2. There is a small amount of $Na_2I^+$ fragment formed even when no water was added to the reaction cell. This is believed to be due to the presence of background water vapor. When the water pressure is carefully raised to 0.06 Torr, the dissolution species $Na_2I^+(H_2O)_x$ with as many as four $H_2O$ molecules are observed. This observation indicates that the hydrated $Na_3I_2^+(H_2O)_m$ adducts prefer to lose a neutral NaI unit, instead of ionic $Na^+$, during the dissolution process. When the water pressure is increased to 0.28 Torr, the spectrum is dominated by $Na_2I^+(H_2O)_x$ fragments. The $Na_2I^+(H_2O)_6$ adduct is clearly seen and subsequent dissolution of the $Na_2I^+(H_2O)_x$ fragments to form predominantly $Na^+(H_2O)_4$ is observed. When the water pressure is raised to 0.49 Torr, the spectrum is dominated by the $Na_2I^+(H_2O)_x$ series of ions and further dissolution is observed with the increased formation of $Na^+(H_2O)_{3,4,5}$.

The experiments described above were performed at various temperatures from 250 to 600 K. These experiments yielded the data necessary for construction of the $\Delta G_T^0$ vs $T$ plot for reaction 1. Information about the solvation dynamics can also be obtained from the mass spectra. Figure 3 shows the spectra for $Na_2I^+$ at various water vapor pressures at 540 K. At this temperature, the equilibrium for $Na_2I^+$ reacting with $H_2O$ favors the reactant side and only one $H_2O$ molecule clustering to the $Na_2I^+$ ion is observed. No dissolution species $Na^+(H_2O)_x$ were observed. The indication here is obvious: the precursors leading to the dissolution of $Na_2I^+(H_2O)_m$ are unable to form at this

(33) (*a*) Chesnavich, W. J.; Bowers, M. T. *Prog. React. Kinet.* **1982**, *11*, 137. (*b*) Chesnavich, W. J.; Bowers, M. T. *J. Chem. Phys.* **1978**, *68*, 901. (*c*) Chesnavich, W. J.; Bowers, M. T. *J. Am. Chem. Soc.* **1976**, *98*, 8301.
(34) Pechukas, P. In*Dynamics of Molecular Collisions, Part B*; Miller, W. H., Ed.; Plenum Press: New York, 1976.
(35) Forst, W. *Theory of Unimolecular Reactions*; Academic Press: New York, 1973.
(36) Robinson, P. J.; Holbrook, K. A. *Unimolecular Reactions*; Wiley-Interscience: New York, 1972.
(37) Pechukas, P.; Light, J. C.; Rankin, C. *J. Chem. Phys.* **1966**, *44*, 794.
(38) Nikitan, E. *Theor. Exp. Chem., Engl. Transl.* **1965**, *1*, 275.

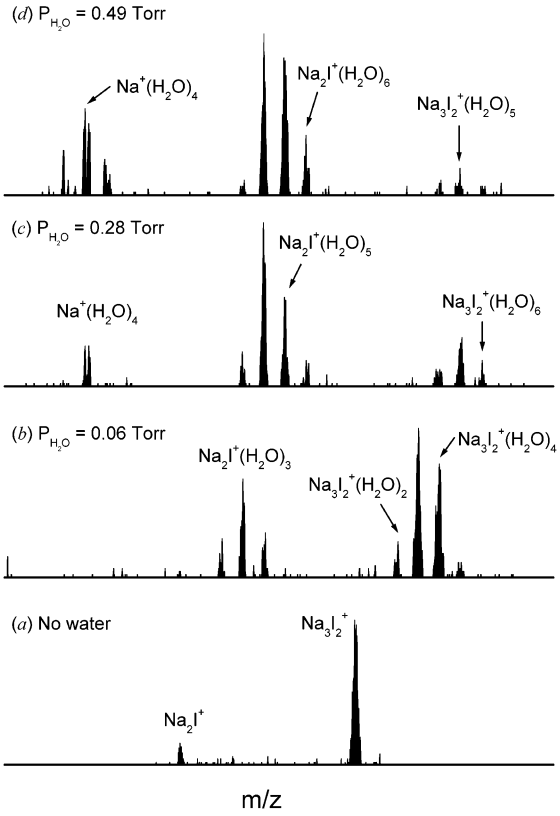


***Figure 2.*** Mass spectra of $Na_3I_2^+$ with different water pressures at room temperature. The dissolution species $Na_2I^+(H_2O)_x$ were observed with only background water vapor. The subsequent dissolution of the $Na_2I^+(H_2O)_x$ adducts occurs when $Na_2I^+(H_2O)_6$ is formed.

high temperature. Similarly, Figure 4 shows the spectra of $Na_3I_2^+$ reacting with $H_2O$ at 440 K. The bottom spectrum shows that only the background water present in the reaction cell is necessary for the dissolution process to occur. The intensities of the $Na_2I^+(H_2O)_x$ species increase and eventually dominate the spectra as the pressure of water increases. However, no subsequent dissolution of the $Na_2I^+(H_2O)_x$ adducts to form $Na^+(H_2O)_y$ species were observed. The dissolution processes of $Na_3I_2^+$ at 300 and 440 K represented by the spectra in Figures 2 and 4, respectively, indicate that only one, or at most two, $H_2O$ molecules are required to dissolve an NaI unit from the $Na_3I_2^+$ ion.

**2. Water Association Energies.** In addition to the dissolution processes of $Na(NaI)_n^+$ by the association of water molecules, equilibrium between $Na(NaI)_n^+$ and $H_2O$ molecules is also established. Figure 5 shows the experimental $\Delta G_T^0$ vs temperature plots for the $Na(NaI)_{n=1,2}^+/H_2O$ association reactions as described in eq 1. A summary of the experimental and theoretical enthalpies and entropies is given in Table 1. The experimental $\Delta S_T^0$ values were taken from the slopes of linear fits to $\Delta G_T^0$ versus temperature plots. The experimental binding energies at 0 K ($D_0 \equiv -\Delta H_0^0$) were obtained from the intercepts, $\Delta H_T^0$, using statistical mechanical fittings.[27]

Some optimized DFT geometries of the $Na_2I^+(H_2O)_m$ ($m = 2-8$) adducts and the $Na_3I_2^+(H_2O)_2$ adduct are displayed in Figure 6. With increasing adduct size, it becomes more difficult to identify lowest-energy structures due to the large number of possible isomeric forms. Typically, the $Na_2I^+(H_2O)_m$ adducts were divided into different categories. First of all, we examined the difference in energies between bridged and nonbridged

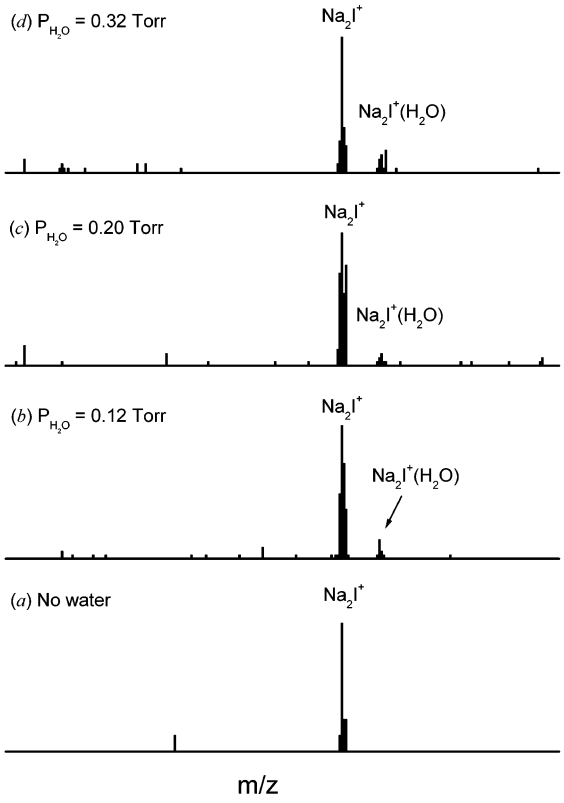


***Figure 3.*** Mass spectra of $Na_2I^+$ with different water pressures at 540 K. No dissolution species $Na^+(H_2O)_x$ were observed at this temperature.

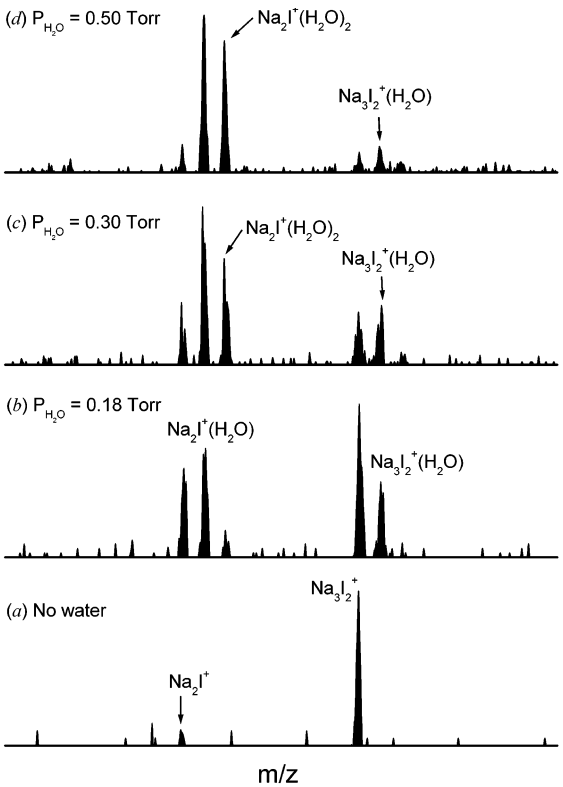


***Figure 4.*** Mass spectra of $Na_3I_2^+$ with different water pressures at 440 K. Dissolution of $Na_3I_2^+$ takes place at all water pressures. No subsequent dissolution of the $Na_2I^+(H_2O)_x$ adducts to form $Na^+(H_2O)_y$ species is found at this temperature.

structures. In the nonbridged structures, all water molecules were considered to cluster to the $Na^+$ cores directly. In the bridged

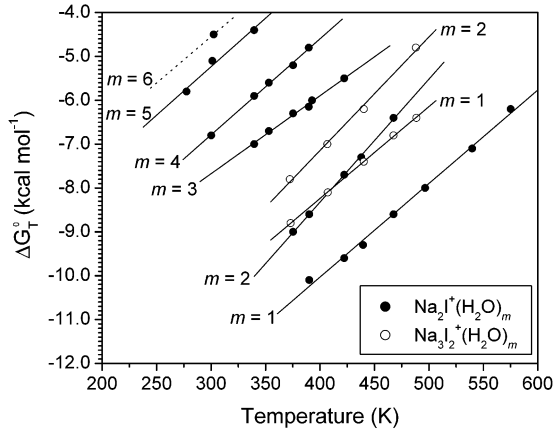


***Figure 5.*** Plots of experimental $\Delta G_T^0$ vs temperature for successive association reactions of $H_2O$ to $Na_2I^+$ and $Na_3I_2^+$ ions (reaction 1). The filled circles are data for the $Na_2I^+(H_2O)_m$ adducts and the open circles are data for the $Na_3I_2^+(H_2O)_m$ adducts.

***Table 1.*** Experimental and Theoretical Enthalpies and Entropies for the Salt−Water Association Reactions $Na(NaI)_n^+(H_2O)_{m-1} + H_2O \rightleftarrows Na(NaI)_n^+(H_2O)_m$

| | | experimental | | theoretical | |
|---|---|---|---|---|---|
| *n* | *m* | $-\Delta H_0^{0\,a}$ | $-\Delta S_T^{0\,b}$ | $-\Delta H_0^{0\,a}$ | $-\Delta S_T^{0\,b,c}$ |
| 1 | 1 | 19.3 | 22.2 | 18.3 | 22.0 |
| | 2 | 19.2 | 28.0 | 17.8 | 27.6 |
| | 3 | 13.4 | 17.8 | 13.6 | 20.5 |
| | 4 | 13.6 | 21.1 | 13.5 | 32.5 |
| | 5 | 11.8 | 22.1 | 11.1 | 22.0 |
| | 6 | ~ 11 | ~ 20 | 11.2 | 22.6 |
| 2 | 1 | 16.7 | 21.0 | 17.2 | 22.3 |
| | 2 | 17.8 | 25.9 | 17.1 | 28.2 |

[a] kcal mol$^{-1}$. Experimental uncertainty ±1 kcal mol$^{-1}$. [b] cal mol$^{-1}$ K$^{-1}$. Valid for temperature range shown in Figure 5. [c] For mean experimental temperature.

structures, some water molecules cluster to the $Na^+$ cores directly and the others form bridges from these directly clustered water molecules to the iodine center. Generally, the bridged adducts are much higher in energy than the nonbridged adducts and hence play marginal roles during hydration. For example, the bridged isomer of $Na_2I^+(H_2O)_4$ adduct is 15.0 kcal mol$^{-1}$ higher in energy than the lowest-energy structure we identified (structure **5** in Figure 6). Also for large $Na_2I^+(H_2O)_m$ adducts, various ways to distribute the $m$ $H_2O$ molecules between the two $Na^+$ centers were considered. The way the $H_2O$ molecules are divided turns out to be crucial in determining whether the cluster is a CIP or an SSIP. For a given $m$ distribution, few symmetry restrictions were imposed and various $H_2O$ orientations were taken into account even for large $Na_2I^+(H_2O)_m$ adducts.

Table 1 shows that the experimental and theoretical binding energies for the $Na_2I^+(H_2O)_{m-1} + H_2O$ ($m = 1-6$) and $Na_3I_2^+(H_2O)_{m-1} + H_2O$ ($m = 1$ and 2) association reactions are in very good agreement. The theoretical $\Delta H_0^0$ values listed include the ZPE and BSSE corrections. The basis of a single water molecule causes a superposition energy of about 0.1 kcal mol$^{-1}$ for all the species involved in this work. The basis from the massive $Na(NaI)_n^+(H_2O)_{m-1}$ group in the $Na(NaI)_n^+(H_2O)_m$ cluster leads to an overestimation in binding energy by 1.0 kcal mol$^{-1}$. As a result, the overall BSSE is approximately 1.0−1.1 kcal mol$^{-1}$ for the successive clustering of each $H_2O$ molecule. The theoretical $\Delta S_T^0$ values for the association of the first two water molecules to the $Na_2I^+$ and $Na_3I_2^+$ ions are also in very good agreement with experiment. The entropy change for the association of the second water molecule is significantly larger than the first. This difference reflects the relatively small rotational entropy, $S_{T,r}^0$, of $Na(NaI)_n^+$ compared to the $Na(NaI)_n^+(H_2O)$ and $Na(NaI)_n^+(H_2O)_2$ adducts. Statistical mechanics shows that the rotational entropies for $Na_2I^+$, $Na_2I^+(H_2O)$, and $Na_2I^+(H_2O)_2$ under 400 K are 19.32, 24.59, and 24.90 cal mol$^{-1}$ K$^{-1}$, respectively. The overall change in rotational entropy for the addition of a water molecule depends on the difference in $S_{T,r}^0$ for the $Na(NaI)_n^+(H_2O)_{m-1}$ reactant and the $Na(NaI)_n^+(H_2O)_m$ product. A smaller rotational entropy for $Na(NaI)_n^+(H_2O)_{m-1}$ leads to a less negative $\Delta S_{T,r}^0$ for the reaction. The theoretical $\Delta S_T^0$ for the association of the third $H_2O$ molecule is noticeably greater than the experimental value, and the deviation increases further for the association of the fourth $H_2O$ molecule. The disagreement between the experimental and the theoretical entropies for the larger clusters is due to the uncertainty of low vibrational frequencies determined by DFT calculations.

The binding energies decrease gradually with the increase in the number of associated water molecules. One remarkable feature for these water association reactions is the pairwise behavior they exhibit. For $Na_2I^+(H_2O)_{1,2}$, the water association energies are approximately 19 kcal mol$^{-1}$. For $Na_2I^+(H_2O)_{3,4}$, the association energies are both nearly 6 kcal mol$^{-1}$ weaker than the first two. For $Na_2I^+(H_2O)_{5,6}$, the binding energies drop down by another 2 kcal mol$^{-1}$. The $Na_2I^+(H_2O)_6$ adduct was only observed below approximately 325 K in our experiment. Because of this and other experimental conditions, only one reliable value for $\Delta G_T^0$ could be obtained for this adduct. To determine an estimate for $\Delta H_0^0$ of $Na_2I^+(H_2O)_6$, $\Delta S_T^0$ was assumed to be −20 cal mol$^{-1}$ K$^{-1}$ based on the values of $\Delta S_T^0$ for $m = 1-5$. This results in a value of −11 kcal mol$^{-1}$ for $\Delta H_0^0$, in line with the pairwise behavior observed for $m = 1-5$. The DFT calculations show both the $Na_2I^+(H_2O)_2$ ion (structure **1** in Figure 6) and $Na_3I_2^+(H_2O)_2$ ion (structure **2** in Figure 6) are linear with two water molecules added on opposite sides of the salt center. The lowest-energy state of the $Na_2I^+(H_2O)_4$ ion has a $D_{2d}$ symmetry with two water molecules clustering to each of the two sodium atoms (structure **5** in Figure 6). The lowest-energy $Na_2I^+(H_2O)_6$ ion has $C_{2h}$ symmetry with three water molecules clustering to each sodium center (structure **9** in Figure 6). The symmetric association of water molecules to the salt clusters leads to the pairwise behavior revealed in $\Delta H_0^0$. The reduction in water association energies with increasing ligand number is primarily due to ligand−ligand repulsion of the water molecules.

It is interesting to compare the water association energies of the $Na^+$, $Na_2I^+$, and $Na_3I_2^+$ ions. The bare $Na^+$ system has been investigated both experimentally[7] and theoretically[8] by a number of research groups. The experimental studies result in an average[39] binding energy of 23.4 kcal mol$^{-1}$ for the first and 19.7 kcal mol$^{-1}$ for the second water molecule. The theoretical studies give average binding energies of 24.7 and 22.1 kcal mol$^{-1}$ for the first and second waters, respectively. Our current

(39) The average binding energies of 23.4 kcal mol$^{-1}$ for the first and 19.7 kcal mol$^{-1}$ for the second water molecule to bare $Na^+$ do not include the values measured by Marinelli and Squires (ref 7*b*) because they are significantly lower than those measured by Dalleska et al. (ref 7*a*) and by Dzidic and Kebarle (ref 7*c*).

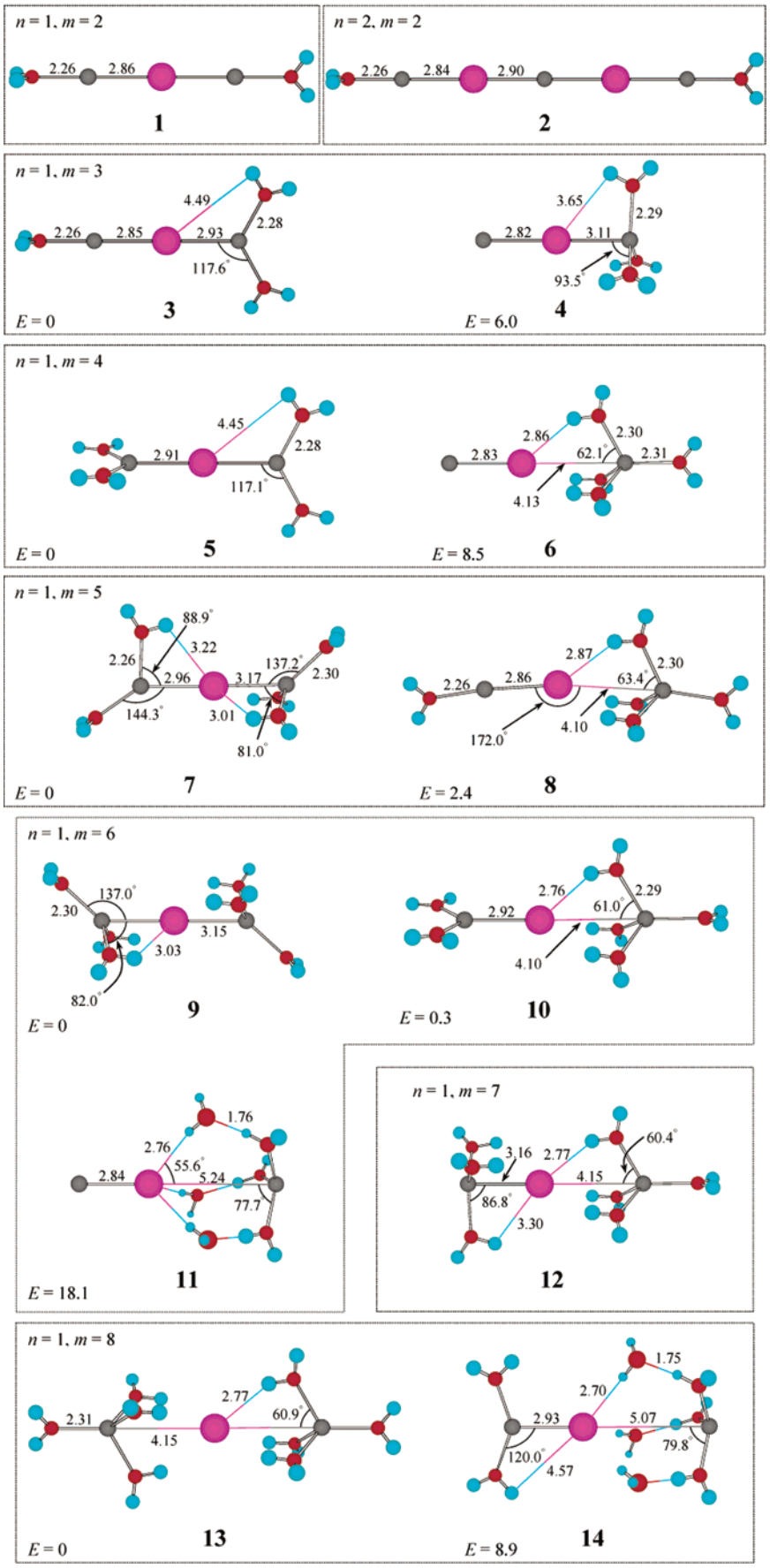


***Figure 6.*** Representative structures for the $Na(NaI)_n^+(H_2O)_m$ ($n = 1$, $m = 2-8$ and $n = 2$, $m = 2$) adducts obtained from DFT. The I-atoms are purple, the Na-atoms gray, the O-atoms red and the H-atoms blue. Selected bond lengths and angles are given in Å and degrees, respectively. For species where more than one isomer is shown ($n = 1$, $m = 3-6$, 8), energies are given in kcal $mol^{-1}$ relative to the lowest-energy structure.

calculations give values of 23.2 and 20.6 kcal mol$^{-1}$ with a BSSE correction of 1.1 kcal mol$^{-1}$ for both $H_2O$ adducts. (The geometry of the $Na^+(H_2O)$ adduct is shown in Supporting Information.) The first water association energies from the DFT calculations are 23.2, 18.3, and 17.2 kcal mol$^{-1}$ for the $Na^+$, $Na_2I^+$, and $Na_3I_2^+$ ions, respectively. The charge−dipole and charge−induced-dipole interactions have the most important contributions to these energies. The DFT calculations indicate positive charges of 0.948, 0.637, and 0.589 on the sodium centers in $Na^+(H_2O)$, $Na_2I^+(H_2O)$ and $Na_3I_2^+(H_2O)$, respectively. This indicates that the water association energies decrease as the charge−dipole interactions decrease. For the neutral $NaI(H_2O)$ adduct, there is no overall charge−dipole interaction but a dipole−dipole interaction is possible. Our DFT calculations give a water association energy of 14.2 kcal mol$^{-1}$ for neutral NaI. This is somewhat surprising because dipole−dipole interactions are usually of the magnitude of several kcal mol$^{-1}$. Two factors, charge separation and geometry, account for the high NaI−$H_2O$ binding energy. The DFT calculations specify a charge on the sodium center in the $NaI(H_2O)$ adduct of 0.642, indicating that NaI is highly ionic. In addition, the $NaI(H_2O)$ adduct has a planar $C_s$ symmetry with the oxygen atom oriented toward the sodium center and one hydrogen atom oriented toward the iodine center, resulting in a quadrupole charge interaction (geometry shown in Supporting Information).

**3. Geometries: CIP and SSIP.** Two components contribute to the enthalpy for reaction 1 measured in this experiment: the energy gained by the association of water molecules with the reactant ion and the energy lost due to the weakening of the Na−I bonds in the product. To analyze the salt−water interactions for the $Na_2I^+$ and $Na_3I_2^+$ systems, we need to compare just the hydration component of $-\Delta H_0^0$ as a function of the number of associated water molecules. Therefore we define the pure hydration energy

$$\Delta E_h(m) = -\Delta H_0^0(m) + \Delta E_{\mathrm{Na-I}}(m) \qquad (9)$$

where $-\Delta H_0^0(m)$ is the total hydration energy calculated for the $Na(NaI)_{1,2}^+$ ion with $m$ associated water molecules and $\Delta E_{\mathrm{Na-I}}(m)$ is the total decrease of the Na−I bond energies with $m$ water molecules clustering to the $Na(NaI)_{1,2}^+$ core. To determine $\Delta E_h(m)$ values using eq 9, theoretical $-\Delta H_0^0(m)$ values were taken from Table 1 and $\Delta E_{\mathrm{Na-I}}(m)$ values were calculated using DFT. Both $\Delta E_h(m)$ and $\Delta E_{\mathrm{Na-I}}(m)$ values are listed in Table 2.

The plots in Figure 7 show the change in the Na−I bond energy of $Na_2I^+$ obtained by varying the Na−I bond distance in the DFT calculations. Three different calculations were performed. First, the bond energy was calculated by varying the two Na−I bond lengths symmetrically. The bond energy was also calculated by varying one of the two Na−I bonds with and without the other Na−I bond optimized. The two curves for asymmetric bond variance almost overlap. This is not surprising since the optimized Na−I bond varies no more than 0.05 Å from the equilibrium position for the range from 1.6 to 5.2 Å of this plot and because the change in bond energy at R(eq) ± 0.05 Å is approximately 0.1 kcal mol$^{-1}$. Figure 7 also shows that symmetric Na−I bond cleavage in $Na_2I^+$ requires more than twice as much energy as asymmetric bond cleavage. The NaI−$Na^+$ bond energy is 39.5 kcal mol$^{-1}$. However, it takes 119.2 kcal mol$^{-1}$ to break NaI apart into $Na^+$ and $I^-$. The symmetric elongation of the bonds in $Na^+-I^--Na^+$ results in more charge separation than in the asymmetric cleavage and hence requires more energy.

One interesting aspect of the salt dissolution processes is the variation in charge separation in alkali halides with the number of associated $H_2O$ molecules. For instance, the charge on the Na center in an isolated NaI molecule is 0.557 according to the Mulliken charge population from the GAUSSIAN98 program. The charge on an isolated $Na^+$ ion is +1. Thus, there is a difference of 0.443 between isolated $Na^+$ and Na in NaI. For a hydrated salt cluster ion, $[(H_2O)_y(NaI)_n-Na'(H_2O)_x]^+$, it is convenient to define a similar quantity as

***Table 2.*** Properties of the Salt−Water Adducts, $Na(NaI)_n^+(H_2O)_m$[a] from DFT Calculations (geometries shown in Figure 6)

| | structure ($m$ $x$ $y$) | $E$[b,c] | $\Delta E_{\mathrm{Na-I}}(m)$[b,d] | $\Delta E_h(m)$[b,e] | $R_{Na'-I}$[f] | $q_{Na'}$[g] | $\Delta q$[h] |
|---|---|---|---|---|---|---|---|
| $n = 1$ | $Na_2I^+$ (0 0 0) | 0 | 0 | 0 | 2.85 | 0.592 | 0.408 |
| | **1** (2 1 1) | 0 | 0.0 | 36.1 | 2.86 | 0.558 | 0.390 |
| | **3** (3 2 1) | 0 | 0.2 | 49.9 | 2.93 | 0.656 | 0.238 |
| | **4** (3 3 0) | 6.0 | 1.7 | 45.4 | 3.11 | 0.670 | 0.206 |
| | **5** (4 2 2) | 0 | 0.6 | 63.8 | 2.91 | 0.660 | 0.234 |
| | **6** (4 4 0) | 8.5 | 15.1 | 70.8 | 4.13 | 0.746 | 0.075 |
| | **7** (5 3 2) | 0 | 2.9 | 77.0 | 3.17 | 0.725 | 0.151 |
| | **8** (5 4 1) | 2.4 | 15.2 | 86.8 | 4.10 | 0.744 | 0.077 |
| | **9** (6 3 3) | 0 | 4.4 | 88.9 | 3.15 | 0.730 | 0.146 |
| | **10** (6 4 2) | 0.3 | 15.3 | 101.5 | 4.10 | 0.741 | 0.080 |
| | **11** (6 6 0) | 18.1 | 24.4 | 92.7 | 5.24 | 0.803 | 0.039 |
| | **12** (7 4 3) | 0 | 19.1 | 113.5 | 4.15 | 0.746 | 0.075 |
| | **13** (8 4 4) | 0 | 35.1 | 140.7 | 4.15 | 0.750 | 0.071 |
| | **14** (8 6 2) | 8.9 | 24.0 | 121.8 | 5.07 | 0.803 | 0.039 |
| $n = 2$ | $Na_3I_2^+$ (0 0 0) | 0 | 0 | 0 | 2.81 | 0.683 | 0.317 |
| | **2** (2 1 1) | 0 | 0.1 | 34.4 | 2.84 | 0.581 | 0.367 |
| $n = 0$ | $Na^+$ | 0 | | 0 | ∞ | 1.000 | |
| | $Na^+(H_2O)$[i] | 0 | | 23.2 | ∞ | 0.948 | |
| | $Na^+(H_2O)_2$[i] | 0 | | 43.9 | ∞ | 0.894 | |
| | $Na^+(H_2O)_3$[i] | 0 | | 60.2 | ∞ | 0.876 | |
| | $Na^+(H_2O)_4$[i] | 0 | | 73.2 | ∞ | 0.821 | |
| | $Na^+(H_2O)_5$[i] | 0 | | 83.6 | ∞ | 0.812 | |
| | $Na^+(H_2O)_6$[i] | 0 | | 93.7 | ∞ | 0.842 | |

[a] $[(H_2O)_y(NaI)_n-Na'(H_2O)_x]^+$, where $m = x + y$. [b] In units of kcal mol$^{-1}$. [c] Energy relative to the lowest-energy state. [d] Decrease in Na−I interionic bond energy. [e] Pure hydration energy as defined in eq 9. [f] Na′−I bond length in Å. [g] Mulliken charge population on the leaving Na′ center as described in eq 10. [h] Difference in charge on Na center in $[Na(H_2O)_x]^+$ and Na′ in $[(H_2O)_y(NaI)_n-Na'(H_2O)_x]^+$ as defined in eq 10. [i] Geometries are shown in Supporting Information.

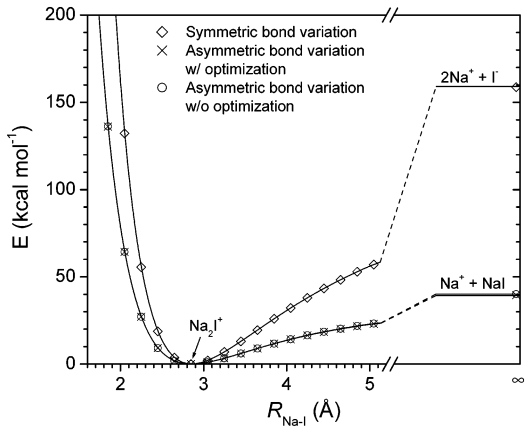


***Figure 7.*** Relative energies of the $Na_2I^+$ ion as a function of the Na−I bond distances obtained from DFT. The diamond symbols were obtained by symmetrically varying both of the Na−I bonds. The cross symbols and the circle symbols were obtained by varying one of the two Na−I bonds with and without the other Na−I bond optimized, respectively.

$$\Delta q = q_{Na} - q_{Na'} \quad (10)$$

where $q_{Na}$ is the charge on the Na center in an isolated $[Na(H_2O)_x]^+$ ion and $q_{Na'}$ is the Mulliken charge on the Na′ center that is being dissolved in the cluster. The quantity $\Delta q$ is presented in Table 2.

Structures for the $Na_2I^+(H_2O)_{n=2-8}$ ions are shown in Figure 6. The lowest-energy $Na_2I^+(H_2O)_2$ structure is linear with two water molecules added to the two sodium centers at the ends (structure **1** in Figure 6). The Na−I bonds are almost intact with a bond distance of 2.86 Å (also see Table 2). The Mulliken charge population shows that there is a 0.558 positive charge on the sodium centers in $Na_2I^+(H_2O)_2$. The charge on Na in $Na^+(H_2O)_2$ is 0.948. Using eq 10 gives $\Delta q = 0.390$, a drop from $\Delta q = 0.443$ for NaI. This structure for $Na_2I^+(H_2O)_2$ corresponds to a CIP with no water molecules lying between the $Na^+$ and $I^-$ ions.[22] The lowest-energy $Na_2I^+(H_2O)_3$ structure has a $C_{2v}$ symmetry with one water molecule clustering to one sodium center and two to the other (structure **3** in Figure 6). The distance of the $[(H_2O)NaI-Na(H_2O)_2]^+$ bond is 2.93 Å, 0.08 Å longer than the $[(H_2O)Na-INa(H_2O)_2]^+$ bond. An isomer of $Na_2I^+(H_2O)_3$ (structure **4**) has all three $H_2O$ molecules clustering to one sodium center and lies 6.0 kcal mol$^{-1}$ higher in energy than structure **3**. The $[NaI-Na(H_2O)_3]^+$ bond is elongated to 3.11 Å and the loss of the Na−I−Na backbone energy is 1.7 kcal mol$^{-1}$. The I• • •HOH bond distances are 3.65 Å, showing a tendency to form I• • •HOH bonds.

The lowest-energy $Na_2I^+(H_2O)_4$ structure has a $D_{2d}$ symmetry with two water molecules clustering to each sodium center (structure **5** in Figure 6). The Na−I bond is elongated by 0.05 Å with respect to $Na_2I^+(H_2O)_2$. This structure is also a CIP since all the water molecules lie at the outer edge of the $Na_2I^+$ core. The Mulliken charge on the sodium center increases to 0.660 and $\Delta q$ is reduced to 0.234, significantly closer to the dissolved state (where $\Delta q = 0$) than $Na_2I^+(H_2O)_2$. In addition to the CIP, another stable structure has been characterized. This species, shown as structure **6** in Figure 6, lies 8.5 kcal mol$^{-1}$ higher in energy than the global ground state (structure **5**), and hence is energetically unfavored. In this structure, all four water molecules cluster to a single sodium atom at one end. Three out of the four water molecules lie between the sodium and iodine centers with their oxygen atoms oriented to the sodium center and one of their hydrogen atoms pointing to the iodine center. Three aspects of this structure allow us to classify it as an SSIP. First, the hydrated sodium and iodine centers are separated by 4.13 Å, 1.22 Å farther apart than in the CIP structure **5** and 1.01 Å farther apart than in structure **4**. The electron-density isosurface[40] plotted in Figure 8*a* shows that the hydrated sodium center is well separated from the iodine while the other $Na^+$ binds tightly to the $I^-$ forming a CIP. Second, the charge on the solvated sodium center increases to 0.746 and $\Delta q$ is 0.075, indicating a substantial separation of charge between sodium and iodine. Third, the loss in the Na−I binding energy is 15.1 kcal mol$^{-1}$ for this structure compared to $Na_2I^+$, whereas the corresponding quantities are only 1.7 and 0.6 kcal mol$^{-1}$ for structure **4** and **5**. The pure hydration energy for structure **6** is 70.8 kcal mol$^{-1}$, which is 7.0 kcal mol$^{-1}$ greater than the lowest-energy species (structure **5**). One might conclude that the increase in hydration energy is due to the stabilization between the iodine and the hydrogen atoms of the $H_2O$ ligands. However, the electron-density isosurface plotted in Figure 8*a* shows there is little overlap of the electron population between the iodine atom and the hydrogen atoms. The calculations show that the $NaI-Na^+$ backbone in this structure is bound by 24.4 kcal mol$^{-1}$ and the diabatic $NaI-Na^+(H_2O)_4$ bond dissociation energy is 26.4 kcal mol$^{-1}$. To dissociate $NaI-Na^+(H_2O)_4$ into NaI and $Na^+(H_2O)_4$, one Na−I bond and three I• • •HOH bonds need to be broken. Therefore, the stabilization energy for each I• • •HOH bond is slightly less than 0.7 kcal mol$^{-1}$. As a comparison, the NaI• • •HOH binding energy is calculated to be 0.6 kcal mol$^{-1}$ for NaI and $H_2O$ with the same orientation. By subtracting the I• • •HOH binding energy, the hydration energy for water molecules associating to the $Na^+$ center in structure **6** is still 5.0 kcal mol$^{-1}$ greater than that in structure **5**. Structure **6** has a much bigger charge separation than structure **5** and hence has a stronger $Na^+-H_2O$ bond. Therefore, the SSIP structure increases the hydration energy in two ways: (1) by having stronger $Na^+-H_2O$ bonds and (2) by introducing the I• • •HOH bonds.

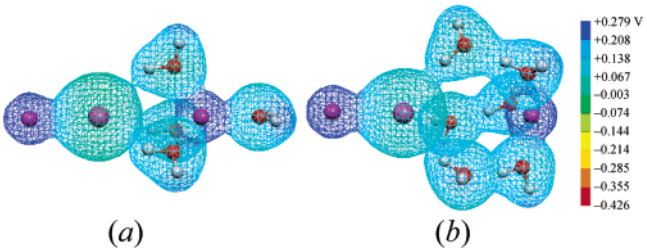


***Figure 8.*** Plots of the electron-density isosurface for (a) the 4-$H_2O$-solvated $Na_2I^+(H_2O)_4$ adduct and (b) the 6-$H_2O$-solvated $Na_2I^+(H_2O)_6$ adduct. The Na-atoms and I-atoms are both purple. The color legend of electrostatic potential is shown on the right.

The lowest-energy structure for $Na_2I^+(H_2O)_5$ is shown as structure **7** in Figure 6. The distance of the $[(H_2O)_2NaI-Na(H_2O)_3]^+$ bond is 3.17 and 2.96 Å for the $[(H_2O)_2Na-INa(H_2O)_3]^+$ bond. Structure **8** is another stable geometry characterized by four $H_2O$ molecules clustering to one of the two sodium centers and one $H_2O$ molecule to the other sodium center. The energy of structure **8** is 2.4 kcal mol$^{-1}$ higher than structure **7**. This energy difference corresponds to the preferential formation of species **7** at a factor of approximately 50 to 1 over formation of species **8** in the 275−300 K temperature range. Thus, DFT results indicate that the $Na_2I^+(H_2O)_5$ observed in our experiment is predominantly a species with a structure like that shown for **7** in Figure 6.

The lowest-energy structure for $Na_2I^+(H_2O)_6$ is shown as structure **9** in Figure 6. Each sodium center has three water molecules clustered to it. Two of the water molecules on each Na center are oriented so one of their hydrogen atoms is coordinated to the iodine center. This structure is classified as a CIP with the Na−I bonds slightly elongated by 0.30 Å to 3.15 Å compared to bare $Na_2I^+$. Structure **10** in Figure 6 is almost isoenergetic to the lowest-energy $Na_2I^+(H_2O)_6$ species, only 0.3 kcal mol$^{-1}$ higher in energy, indicating structures **9** and **10** equally contributes under our experimental conditions. In structure **10**, one of the sodium centers is solvated by four water molecules and forms an SSIP with the iodine, while the other sodium is solvated by two water molecules and forms a CIP with the iodine. Therefore, overall, structure **10** is classified

(40) Flükiger, P.; Lüthi, H. P.; Portmann, S.; Weber, J. *MOLEKEL 4.0*; Swiss Center for Scientific Computing: Manno (Switzerland), 2000.

***Table 3.*** Energetics and Efficiencies for the Reaction $Na(NaI)^{+}_{n=1,2}(H_2O)_{x+y-1} + H_2O \xrightarrow{k_{expt}(T)} Na(NaI)^{+}_{n=0,1}(H_2O)_x + (NaI)(H_2O)_y$[a]

| reactants | products | $\Delta H^0_0$ (kcal mol$^{-1}$) [b] | reaction efficiency $\omega(T = 300)$ [c] | extent of reaction [d] |
|---|---|---|---|---|
| $Na_2I^+ + H_2O$ | $Na^+(H_2O) + NaI$ | 15.8 | $2.9 \times 10^{-8}$ | 0.00 |
| $Na_2I^+(H_2O) + H_2O$ | $Na^+(H_2O)_2 + NaI$ | 13.5 | $2.1 \times 10^{-6}$ | 0.01 |
| $Na_2I^+(H_2O)_2 + H_2O$ | $Na^+(H_2O)_3 + NaI$ | 15.2 | $1.6 \times 10^{-7}$ | 0.00 |
| $Na_2I^+(H_2O)_3 + H_2O$ | $Na^+(H_2O)_4 + NaI$ | 15.9 | $2.7 \times 10^{-7}$ | 0.00 |
| $Na_2I^+(H_2O)_4 + H_2O$ | $Na^+(H_2O)_4 + NaI(H_2O)$ | 14.7 | $1.1 \times 10^{-6}$ | 0.01 |
| $Na_2I^+(H_2O)_5 + H_2O$ | $Na^+(H_2O)_4 + NaI(H_2O)_2$ | 12.7 | $2.8 \times 10^{-5}$ | 0.17 |
| $Na_2I^+(H_2O)_6 + H_2O$ | $Na^+(H_2O)_4 + NaI(H_2O)_3$ | 12.1 | $2.5 \times 10^{-5}$ | 0.15 |
| $Na_2I^+(H_2O)_7 + H_2O$ | $Na^+(H_2O)_5 + NaI(H_2O)_3$ | 11.8 | $2.3 \times 10^{-5}$ | 0.14 |
| | $Na^+(H_2O)_6 + NaI(H_2O)_2$ | 13.2 | $6.6 \times 10^{-6}$ | 0.04 |
| | $Na^+(H_2O)_4 + NaI(H_2O)_4$ | 13.2 | $3.8 \times 10^{-6}$ | 0.02 |
| $Na_3I_2^+ + H_2O$ | $Na_2I^+(H_2O) + NaI$ | 10.2 | $5.9 \times 10^{-5}$ | 0.32 |
| $Na_3I_2^+(H_2O) + H_2O$ | $Na_2I^+(H_2O)_2 + NaI$ | 9.6 | $1.8 \times 10^{-4}$ | 0.69 |

[a] Geometries of the neutral $(NaI)(H_2O)_y$ species are shown in Supporting Information. [b] From DFT calculations. [c] Defined in eq 7. Details of the efficiency calculations can be found in Supporting Information. [d] Calculated with eq 8 using $t = 1$ ms, $P_{H_2O} = 0.3$ Torr and $T = 300$ K.

as an SSIP. A comparison of the symmetric 3-$H_2O$-ligated structure (**9** in Figure 6) and the asymmetric 4,2-$H_2O$-ligated structure (**10** in Figure 6) shows that the Na−I bond energy in the SSIP species is decreased by 11 kcal mol$^{-1}$ (see Table 2), indicating that shifting one $H_2O$ ligand results in a major change in the Na−I bond strength. In addition to this 4-$H_2O$-molecule-solvated SSIP, a second SSIP structure exists for $Na_2I^+(H_2O)_6$. This SSIP has six water molecules between one of the sodium ions and the iodine center (structure **11** in Figure 6), a structure analogous to the SSIP of $NaCl(H_2O)_6$ found by Jungwirth.[16] The second $Na_2I^+(H_2O)_6$ SSIP differs from structure **10** in that it has hydrogen bond bridges between water molecules. Three water molecules cluster to one sodium center and the other three cluster to the iodine center. These two sets of water molecules are then connected via H• • •O• • •H hydrogen bonds. The isosurface wrapping of the electron density is shown in Figure 8*b*. The separation of the sodium ion and the iodine center, as well as the I• • •O• • •H bonding are clearly shown in this depiction. Although the second SSIP (structure **11**) is a stable local minimum, it lies 18.1 kcal mol$^{-1}$ higher in energy than the lowest-energy state and thus is significantly energetically unfavored compared to both structures **9** and **10**. In this second SSIP, the solvated sodium center is separated from iodine by 5.24 Å, 1.14 Å more than in the 4-$H_2O$-solvated SSIP, structure **10**. The charge on the solvated sodium ion in **11** is 0.803, corresponding to a $\Delta q$ of 0.039.

The optimized structure of $Na_2I^+(H_2O)_7$ is shown as structure **12** in Figure 6. Four $H_2O$ molecules solvate an $Na^+$ center and form an SSIP to the iodine center. It is interesting to note that all three water molecules clustering to the sodium atom on the left in **12** angle into the iodine center, unlike the $Na_2I^+(H_2O)_6$ adduct, where one water molecule on each sodium atom is on the outer edge of the Na−I−Na core. Mulliken population analysis shows that the charge on the iodine center is −0.664 for the $Na_2I^+(H_2O)_7$ adduct and −0.544 for the $Na_2I^+(H_2O)_6$ adduct. The separation of charge achieved by forming the SSIP in the $Na_2I^+(H_2O)_7$ adduct also helps induce the ionic character in the iodine center. Water molecules are attracted toward the iodine center, resulting in an $NaI-(H_2O)_3$ CIP within the overall structure of **12** analogous to the lowest-energy $NaI(H_2O)_3$ species (structure shown in Supporting Information). Two optimized structures of $Na_2I^+(H_2O)_8$ are shown as structures **13** and **14** in Figure 6. For the lowest-energy structure **13**, four water molecules solvate each of the two sodium cations, forming two sets of $Na^+-I^-$ pairs, and the iodine center is stabilized by six water

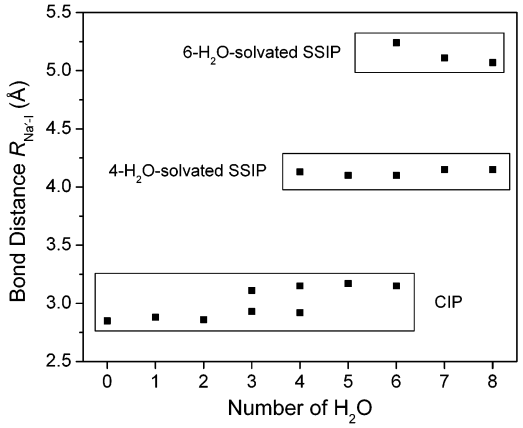


***Figure 9.*** Variation of the Na′−I bond distances from DFT in the $[(H_2O)_yNaI-Na'(H_2O)_x]^+$ adducts with total number of associated water molecules $m = x + y$ for $m = 0-8$. Three separate zones from bottom to top correspond to the CIP, 4-$H_2O$-solvated SSIP and 6-$H_2O$-solvated SSIP.

molecules. Considering the loss of Na−I binding energy, it is energetically unfavorable to elongate both of the Na−I bonds symmetrically (Figure 7) relative to unsymmetrical extension. The loss of Na−I binding energy is 35.1 kcal mol$^{-1}$ for structure **13**. However, the iodine center has a much stronger ionic character compared to the asymmetrically extended structures (**6**, **8**, **10**, and **12**). As a consequence, the $I^-{-}H_2O$ bond strength is enhanced dramatically, resulting in a binding energy of 13.9 kcal mol$^{-1}$ for these six $I^-{-}H_2O$ bonds in $I^-(H_2O)_6$. The net result is that addition of the eighth water molecule to $Na_2I^+(H_2O)_7$, which is a 4,3-$H_2O$-ligated structure, has a significant binding energy (10 kcal mol$^{-1}$ from DFT). Structure **14** is in the 6,2 water configuration. It has a larger Na−I separation for the hexasolvated sodium center and lies 8.9 kcal mol$^{-1}$ higher in energy than structure **13**. This SSIP structure is analogous to structure **11** in that they both have one long Na−I bond and extensive charge separation (small $\Delta q$).

The trend of migrating from CIP to 4-$H_2O$-solvated SSIP and to 6-$H_2O$-solvated SSIP with increased number of associated water molecules is summarized in Figure 9. Three separate zones are clearly shown in this plot of Na−I bond distance versus number of water molecules. The 4-$H_2O$-solvated SSIP structure appears when four water molecules or more are associated to $Na_2I^+$. The 6-$H_2O$-solvated SSIP structure appears when the number of water molecules reaches six or more. The CIP structure is unfavored when more than six water molecules associate with $Na_2I^+$.

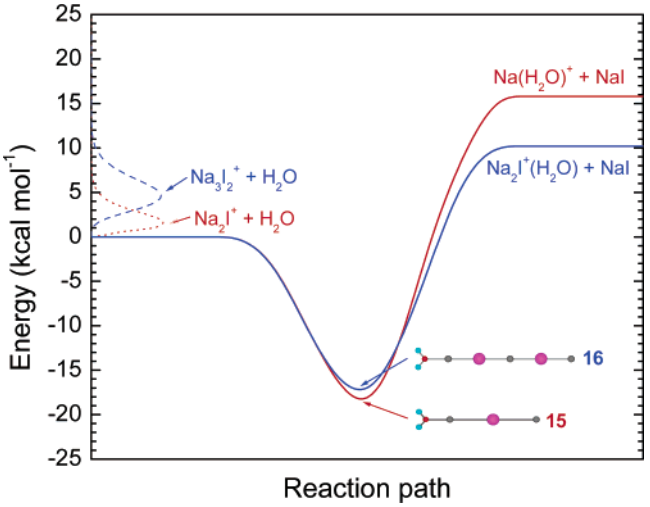


***Figure 10.*** Lowest-energy reaction paths for the association of the first $H_2O$ to $Na_2I^+$ and $Na_3I_2^+$ obtained from DFT. The dotted curve is the Boltzmann energy distribution of the orbiting $Na_2I^+ + H_2O$ reactants. The dashed curve is the Boltzmann energy distribution of the orbiting $Na_2I_2^+ + H_2O$ reactants.

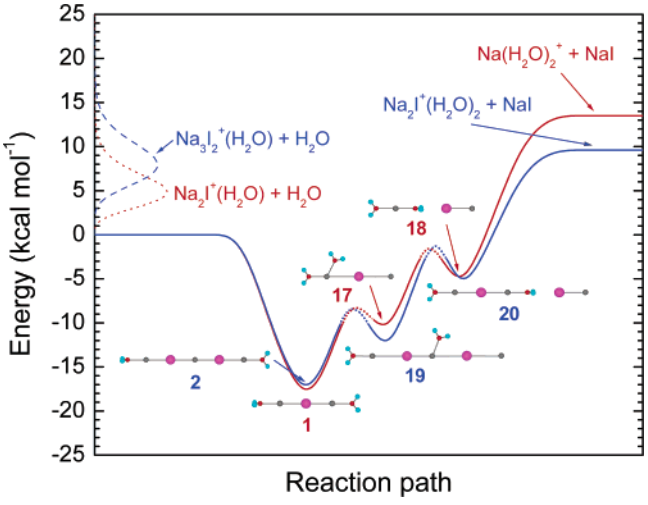


***Figure 11.*** Lowest-energy reaction paths for the association of $H_2O$ to $Na_2I^+(H_2O)$ and $Na_3I_2^+(H_2O)$ obtained from DFT. The Boltzmann energy distributions of the reactants are shown on the left. The structures of intermediate species are indicated along the reaction paths. The energies of the isomerization transition states were not calculated. Therefore, the barriers associated with these states are shown as dotted lines on the reaction-path diagram.

**4. Reaction Paths.** Figure 10 shows the lowest-energy reaction paths calculated by DFT for the association of the first $H_2O$ molecule to $Na_2I^+$ and to $Na_3I_2^+$ (reactions 11 and 12)

$$Na_2I^+ + H_2O \rightarrow Na^+(H_2O) + NaI \qquad (11)$$

$$Na_3I_2^+ + H_2O \rightarrow Na_2I^+(H_2O) + NaI \qquad (12)$$

Formation of $NaI(H_2O)$ is not favored in either the reaction of $Na_2I^+$ or $Na_3I_2^+$ with water because, according to DFT, the binding energy of the neutral NaI to water is only 14.2 kcal $mol^{-1}$, whereas water binds 9.0 and 4.1 kcal $mol^{-1}$ more strongly to ionic $Na^+$ and $Na_2I^+$, respectively. As a result, the $H_2O$ molecule would prefer to stay with the ionic species. The binding energy from DFT is 39.5 kcal $mol^{-1}$ for the $Na^+-NaI$ bond and 29.2 kcal $mol^{-1}$ for the $Na_2I^+-NaI$ bond. Reactions 11 and 12 are endothermic by 15.8 kcal $mol^{-1}$ and 10.2 kcal $mol^{-1}$, respectively. For reaction 11, the efficiency calculated with phase space theory (PST) is $2.9 \times 10^{-8}$. Essentially, all $Na_2I^+ + H_2O$ remain unreacted under our typical experiment conditions (1 ms reaction time, 0.3 Torr water pressure and 300 K temperature). Table 3 summarizes the energetics, reaction efficiencies and extents of reaction for the salt dissolutions given in reaction 6. For the reactions of $Na_2I^+(H_2O)_{0-4}$, the extent of dissolution of the $Na_2I^+$ ion is minor. These calculated reaction efficiencies coincide with the experimental observations shown in Figures 1 to 4.

In contrast, the calculated efficiency for loss of NaI from nascent $Na_3I_2^+(H_2O)$ (reaction 12) is $5.9 \times 10^{-5}$, which corresponds to a 32% extent of reaction. Again, these calculations are in agreement with experimental observations as shown in Figures 2 and 4. It may be considered surprising that we observe reaction 12 experimentally, given that it is 10.2 kcal $mol^{-1}$ endothermic. However, consideration of the Boltzmann energy distribution for the $Na_3I_2^+ + H_2O$ reactants reveals that there is a 1% probability the reactants have energies higher than the product threshold. It is these high-energy reactants that contribute to the small, but significant reaction efficiency of $5.9 \times 10^{-5}$.

For reactants $Na_2I^+(H_2O) + H_2O$ and $Na_3I_2^+(H_2O) + H_2O$, the lowest-energy reaction paths calculated by DFT are shown in Figure 11. Reactions 13 and 14

$$Na_2I^+(H_2O) + H_2O \rightarrow Na^+(H_2O)_2 + NaI \qquad (13)$$

$$Na_3I_2^+(H_2O) + H_2O \rightarrow Na_2I^+(H_2O)_2 + NaI \qquad (14)$$

are 13.5 kcal $mol^{-1}$ and 9.6 kcal $mol^{-1}$ endothermic, respectively. The efficiency for reaction 13 calculated by PST is $2.1 \times 10^{-6}$, which results in a 1% extent of reaction under the experimental conditions specified in Table 3. For reaction 14, the efficiency is calculated to be $1.8 \times 10^{-4}$, which leads to a 69% extent of reaction. The Boltzmann distribution indicates 27% of the $Na_3I_2^+(H_2O) + H_2O$ reactants have energy higher than the threshold for formation of the $Na_2I^+(H_2O)_2 + NaI$ products. The PST calculations show that reactants with energies in the highest 12% of the Boltzmann energy distribution are predominately the ones that go on to form products.

For the $Na_2I^+(H_2O) + H_2O$ system, the product $Na^+(H_2O)_2$ has a linear structure with two water molecules adding on opposite side on sodium center (geometry shown in Supporting Information). To produce this species, a rearrangement of the water molecules to form structure **17** in Figure 11 occurs along the reaction path. This is followed by an $H_2O$ insertion into an Na−I bond to form the SSIP structure **18** which leads to dissociation. The lowest-energy ionic product $Na_2I^+(H_2O)_2$ in reaction 14, has the same structure as the intermediate in reaction 13 (structure **1**). Similar to reaction 13, the $Na_3I_2^+(H_2O) + H_2O$ system includes $H_2O$ migration to form structure **19** followed by a cooperative insertion to form the SSIP structure **20** and dissociation to products. All the intermediates in reactions 13 and 14 have energies lower than the $Na(NaI)_n^+(H_2O) + H_2O$ ($n = 1$ and 2) reactants. Although inclusion of the detailed mechanisms indicated in Figure 11 would have some effect on the PST reaction efficiencies, these effects are expected to be minor and hence were not included in the calculated efficiencies

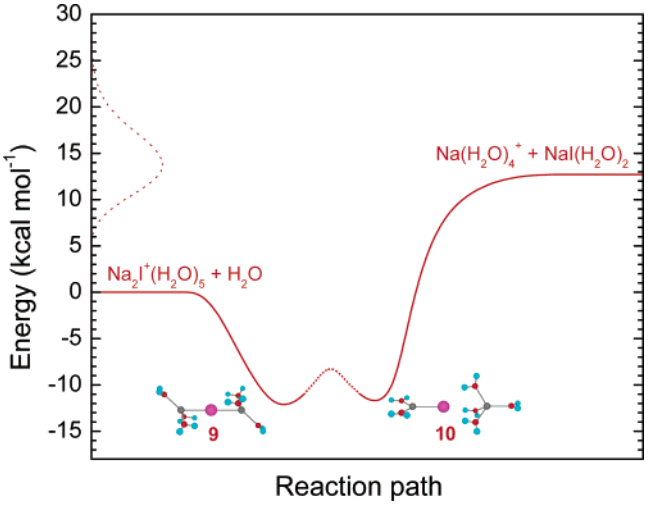


***Figure 12.*** Lowest-energy reaction path for the association of $H_2O$ to $Na_2I^+(H_2O)_5$ obtained from DFT. The 4-$H_2O$-solvated $Na_2I^+(H_2O)_6$ intermediate can dissociate directly to the $Na^+(H_2O)_4 + NaI(H_2O)_2$ products. The energies of the isomerization transition states were not calculated. Therefore, the barriers associated with these states are shown as dotted lines on the reaction-path diagram.

given in Table 3. The approximation used in the PST calculations is adequate to give semiquantitative agreement with the experimental results.[41]

Different reaction pathways without water migration were also considered for reactions 13 and 14. One possibility is that two water molecules cluster to a single sodium center, instead of one migrating and then inserting into the Na−I bond. For the $Na_2I^+$ system, DFT calculations put this $Na_2I^+(H_2O)_2$ adduct 2.6 kcal mol$^{-1}$ higher in energy than the ground-state structure **1** shown in Figure 6. However, the reaction efficiency calculated by PST is not affected at all, since the $Na^+(H_2O)_2$ product remains the same. For the $Na_3I_2^+$ system, the corresponding intermediate is 3.9 kcal mol$^{-1}$ higher in energy than the lowest-energy structure **2**. But unlike the $Na_2I^+$ system, the products of the mechanism involving two water molecules clustering to a single sodium center differ from those shown in Figure 11. Instead of forming $[(H_2O)NaI-Na(H_2O)]^+$, $[NaI-Na(H_2O)_2]^+$ is formed. As mentioned, this isomer is higher in energy by 2.6 kcal mol$^{-1}$, resulting in an endothermicity of 12.2 kcal mol$^{-1}$ for reaction 14. The reaction efficiency for this channel is calculated to be $5.2 \times 10^{-6}$, significantly smaller than the more efficient channel, formation of $[(H_2O)NaI-Na(H_2O)]^+$.

Species resulting from the dissolution processes are only observed when six or more water molecules cluster to an $Na_2I^+$ core (as indicated in Figures 1 and 2). This result is consistent with the reaction efficiencies calculated with PST that the dissolution reaction

$$Na_2I^+(H_2O)_{x+y-1} + H_2O \rightarrow Na^+(H_2O)_x + NaI(H_2O)_y \quad (15)$$

occurs when the number of associated water molecules, $x + y$, is six or more (see Table 3). Figure 12 shows the reaction path for the sixth $H_2O$ molecule associating to $Na_2I^+(H_2O)_5$. The sixth water molecule can cluster to $Na_2I^+(H_2O)_5$ symmetrically, resulting in three $H_2O$ ligands on each sodium atom or asymmetrically with two $H_2O$ molecules associated to one sodium atom and the other four associated to the other sodium atom. These two structures are almost isoenergetic with a water association energy of approximately 12 kcal mol$^{-1}$. The asymmetric adduct **10** has an SSIP structure and can lead to the $Na^+(H_2O)_4 + NaI(H_2O)_2$ products directly. The overall dissolution reaction is 12.7 kcal mol$^{-1}$ endothermic. The calculated reaction efficiency is $2.8 \times 10^{-5}$, which corresponds to a 17% extent of reaction. The endothermicity for the dissolution reaction upon addition of the seventh and the eighth $H_2O$ ligands drops down slightly compared to the sixth $H_2O$. The reaction efficiencies are $2.5 \times 10^{-5}$ and $2.3 \times 10^{-5}$, respectively, similar to the efficiency of dissolution upon addition of the sixth water molecule. The lowest-energy path for the reaction $Na_2I^+(H_2O)_7 + H_2O$ leads to dissolution species of $Na^+(H_2O)_5 + NaI(H_2O)_3$. The dissolution channels producing the products $Na^+(H_2O)_6 + NaI(H_2O)_2$ and $Na^+(H_2O)_4 + NaI(H_2O)_4$ are both more endothermic by 1.4 kcal mol$^{-1}$, resulting in smaller reaction efficiencies.

## Conclusions

(1) Dissolution of $Na_2I^+$ occurs when six $H_2O$ molecules are ligated to the salt cluster. Although the experiment cannot verify which $Na_2I^+(H_2O)_6$ isomer (structures **9** and **10**) produces the dissolution species $Na^+(H_2O)_x$, DFT calculations suggest that the dissolution process takes place via an SSIP species with four $H_2O$ ligands solvating the $Na^+$ center that will leave the cluster, consistent with dissociation of structure **10**.

(2) Dissolution of $Na_3I_2^+$ occurs when only one or two $H_2O$ molecules are ligated to the salt cluster. DFT calculations suggest that a migration followed by insertion of an $H_2O$ ligand into an Na−I bond occurs during the dissolution process of $Na_3I_2^+(H_2O)_2$. The loss of an NaI unit from $Na_3I_2^+$ is the only dissolution channel; loss of $Na^+$ is not observed.

(3) The fact that 6 water molecules are required for solvent-assisted loss of NaI from $Na_2I^+$ and only one or two water molecules for loss of NaI from solvated $Na_3I_2^+$ reflects the difference in energies for binding NaI to $Na^+$ and to $Na_2I^+$, respectively.

(4) Two types of solvent-separated ion pairs for the $Na_2I^+(H_2O)_m$ adducts ($m \geq 4$) were characterized with DFT calculations. One has four $H_2O$ molecules solvating one of the sodium atoms, whereas the second SSIP has six $H_2O$ molecules solvating one sodium atom.

(5) For all the $Na_2I^+(H_2O)_m$ clusters, an increase in charge separation with an increase in the number of $H_2O$ ligands was observed. Theory indicates that four or more water molecules clustered to a single sodium center will lead to an adequate separation of charge for an Na−I SSIP to form.

(6) Experimental sequential association energies and entropies for one through six water molecules clustering to the $Na_2I^+$ ion, and one and two water molecules clustering to the $Na_3I_2^+$ ion are reported. The water association energies show a pairwise behavior, indicating a symmetric association of water molecules to the linear $Na_2I^+$ and $Na_3I_2^+$ ions. This pairwise behavior is well reproduced by DFT calculations.

(7) The association energy of the first water molecule decreases in the order $Na^+$, $Na_2I^+$, and $Na_3I_2^+$, an effect due primarily to reduction of the charge−dipole interaction.

(41) A complete treatment would also require inclusion of an energy transfer mechanism between the bath gas (primarily He) and the nascent $Na(NaI)_{n=1,2}^+(H_2O)_m$ complexes. Inclusion of such a mechanism would decrease the calculated reaction probability (add a term to the denominator in eq 7) but would not change any of the conclusions drawn here.

**Acknowledgment.** We gratefully acknowledge the support of the National Science Foundation under Grant No. CHE-0140215.

**Supporting Information Available:** Details and input parameters for phase space theory calculations. Water association energies for $NaI(H_2O)_{1-4}$ from DFT. Structures of $Na^+(H_2O)_{1-6}$ and $NaI(H_2O)_{1-4}$. This material is available free of charge via the Internet at http://pubs.acs.org.

JA028411Y